HHS Public Access

Author manuscript

Med Devices Sens. Author manuscript; available in PMC 2019 August 21.

Published in final edited form as:

Med Devices Sens. 2018 June ; 1(3): . doi:10.1002/mds3.10018.

High-speed Intraoperative Assessment of Breast Tumor Margins by Multimodal Ultrasound and Photoacoustic Tomography

Rui Li[#1,2,3], **Lu Lan**[#1,9], **Yan Xia**[4], **Pu Wang**[4], **Linda K. Han**[5], **Gary L. Dunnington**[5], **Samilia Obeng-Gyasi**[5], **George E. Sandusky**[6], **Jennifer A. Medley**[7], **Susan T. Crook**[7], **Ji-Xin Cheng**[1,8,9,*]

[1]Weldon School of Biomedical Engineering, Purdue University, 206 S Martin Jischke Dr., West Lafayette, Indiana, 47907, USA.

[2]School of Biological Science and Medical Engineering, Beihang University, Beijing, China, 100083

[3]Beijing Advanced Innovation Center for Biomedical Engineering, Beihang University, Beijing, China, 102402

[4]Vibronix, Inc., 1281 Win Hentschel Blvd., West Lafayette, Indiana, 47906, USA.

[5]Indiana University Health Melvin and Bren Simon Cancer Center, 1030 W. Michigan St., Breast Center, Indianapolis, Indiana 46202, USA.

[6]Department of Pathology & Laboratory Medicine, Indiana University School of Medicine, 350 West 11th Street, Indianapolis, Indiana, 46202, USA.

[7]Department of Radiology and Imaging Sciences, Indiana University School of Medicine, 550 N. University Blvd, Indianapolis, Indiana 46202, USA

[8]Purdue University Center for Cancer Research, 201 S. University Street, West Lafayette, Indiana, 47906, USA.

[9]Photonics Center, Boston University, 8 Saint Mary's Street, Boston, MA 02215, USA

[#] These authors contributed equally to this work.

Abstract

Conventional methods for breast tumor margins assessment need a long turnaround time, which may lead to re-operation for patients undergoing lumpectomy surgeries. Photoacoustic tomography (PAT) has been shown to visualize adipose tissue in small animals and human breast. Here, we demonstrate a customized multimodal ultrasound and PAT system for intraoperative breast tumor margins assessment using fresh lumpectomy specimens from 66 patients. The system provides the margin status of the entire excised tissue within 10 minutes. By subjective reading of three researchers, the results show 85.7% [95% confidence interval (CI), 42.0% - 99.2%] sensitivity and 84.6% (95% CI, 53.7% - 97.3%) specificity, 71.4% (95% CI, 30.3% - 94.9%)

[*]Corresponding author. jxcheng@bu.edu.

Conflict of Interests

Pu Wang, Yan Xia, Linda Han, and Ji-Xin Cheng had a financial interest in Vibronix inc.

sensitivity and 92.3% (95% CI, 62.1% - 99.6%) specificity, and 100% (95% CI, 56.1% - 100%) sensitivity and 53.9% (95% CI, 26.1% - 79.6%) specificity respectively when cross-correlated with post-operational histology. Furthermore, a machine learning-based algorithm is deployed for margin assessment in the challenging ductal carcinoma *in situ* tissues, and achieved 85.5% (95% CI, 75.2% - 92.2%) sensitivity and 90% (95% CI, 79.9% - 95.5%) specificity. Such results present the potential of using mutlimodal ultrasound and PAT as a high-speed and accurate method for intraoperative breast tumor margins evaluation.

Keywords

breast cancer; imaging; margin status; lipid; photoacoustic tomography

1. Introduction

Each year, there are ~249,000 newly-diagnosed breast cancer cases in the United States, 70% of which undergo breast-conserving surgery, or lumpectomy [1]. Compared to mastectomy, lumpectomy when used in conjunction with radiation therapy has equivalent survival outcomes, and is the preferred surgical intervention for early stage breast cancer [2–5]. However, due to failure to achieve clear or negative margins in lumpectomy, 20 – 40% of patients require additional operative intervention in the form of re-excision or mastectomy [6–10]. Therefore, the ability to obtain accurate intraoperative feedback about margin status will reduce the need for re-excision and surgery related cost. Currently, there have been multiple existing or emerging intraoperative imaging tools for breast tumor margin assessment (Table S1). Frozen section and imprint cytology are applied clinically, but they suffer from long procedure time and low sensitivity (70%) due to sampling rate limitation [11–14]. Radio frequency spectroscopy reduces the procedure time, but still suffers from limited sensitivity (70%) and specificity (68%) owning to the lack of chemical selectivity [15,16]. Intraoperative X-ray provides the margin status in depth by displaying two-dimensional projections in several minutes, but the sensitivity (49%) is reported very low due to the poorly-defined tissue boundary [17,18]. The emerging optical technologies, including optical coherence tomography (OCT), Raman spectroscopy, and diffuse reflectance imaging have improved the sensitivity and specificity, but still suffer from long procedure time, inadequate imaging depth, or limited detection area [19–22]. Therefore, an unmet need exists in developing an intraoperative margin assessment tool that is rapid, accurate, and able to measure the entire tissue surface with adequate imaging depth [22,23].

Intraoperative ultrasound has been used as a guiding tool in breast-conserving surgery to locate the tumor position [24]. A recent study demonstrated the feasibility of high frequency ultrasound for intraoperative breast tumor margin assessment with 74% sensitivity and 85% specificity in ductal carcinoma *in situ* [25]. Photoacoustic tomography (PAT), compatible with conventional ultrasonography, has proved its capability in rapid deep tissue imaging with optical absorption contrast and sub millimeter resolution [26,27]. Based on electronic absorption of hemoglobin or exogenous contrast agents, PAT has been used to study brain function, liver diseases, tooth health, and breast tumor margins in mouse models [28–32]. In particular, based on absorption of hemoglobin, PAT has been used to detect breast cancer

due to abnormal angiogenesis in recent clinical studies [33–37]. Also, based on electronic absorption of DNA and RNA, photoacoustic microscopy was performed to analyze the lumpectomy specimen for margin evaluation [38]. More recently, PAT based on the overtone absorption of lipid in the second optical window (Figure S1) has opened up multiple applications including intravascular plaque imaging, peripheral nerve imaging, and etc [39–41]. Because of rich lipid content in the human breast, these previous advancements shed a light on the use of the second-window PAT plus ultrasound for breast tumor margins assessment.

Herein, we demonstrate the first application of a multimodal ultrasound and PAT system for high-speed intraoperative assessment of breast tumor margins with high sensitivity and specificity. By implementing a customized automatic tissue scanner, the system provides a stack of two-dimensional images of the entire tissue surface with 6 mm photoacoustic imaging depth and ~200 μm axial resolution within 10 min. The system outputs two imaging channels: high-frequency ultrasound images showing the tissue morphology, and photoacoustic images indicating lipid distribution, which is the major component of healthy tissue in human breast. In a clinical study of 66 patients, we performed imaging on the whole fresh excised breast tumor tissues, and then correlated it with the corresponding histological results to determine the sensitivity and specificity. By subjective reading of three researchers, the results show 85.7% (95% CI, 42.0% – 99.2%) sensitivity and 84.6% (95% CI, 53.7% – 97.3%) specificity, 71.4% (95% CI, 30.3% – 94.9%) sensitivity and 92.3% (95% CI, 62.1% – 99.6%) specificity, and 100% (95% CI, 56.1% – 100%) sensitivity and 53.9% (95% CI, 26.1% – 79.6%) specificity, respectively. Furthermore, in order to mitigate readers' subjective variation and reduce the reading time, we implement a deep convolutional neural network (CNN) machine learning algorithm to differentiate positive margins from negative margins, specifically for ductal carcinoma in situ, and achieve 85.5% (95% CI, 75.2% – 92.2%) sensitivity and 90% (95% CI, 79.9% – 95.5%) specificity. Together, these results demonstrate the translational potential and intraoperative practicality of multimodal ultrasound and PAT in assessment of breast tumor margins in breast-conserving surgeries.

2. Results and Discussion

2.1. Engineering an intraoperative multimodal ultrasound and PAT system

Using overtone absorption of lipid as contrast, we built a multimodal ultrasound and PAT system capable of fast and automatic detection of ultrasound/photoacoustic signals (Figure 1) with the goal of distinguishing breast cancer from non-cancerous tissue within 2 mm surface in 10 minutes. The system employed a custom-built, all-solid-state Raman laser as the excitation source, since the output wavelength lies in the optical window to solely visualize lipid in the breast [42,43]. The 10 Hz, 10 ns pulse trains with the pulse energy of 100 mJ at 1197 nm wavelength were delivered to the excised breast tissue via a fiber bundle to effectively and sufficiently excite the lipid in the breast tissue to generate photoacoustic signals (Figure S2). The generated photoacoustic signals were acquired by a customized 18 MHz high-frequency ultrasound array with 128 elements and 50% bandwidth. Meanwhile, the same transducer array emits and receives ultrasound signals, which were then processed

by a high-frequency ultrasound imaging system. The laser and the ultrasound system were connected to a computer to synchronize the trigger and visualize the registered ultrasound/photoacoustic images. In order to meet the need of fast intraoperative margin assessment, an automatic tissue scanner (Figure S3) was designed and built based on a series of clinical testing of specimens from a total of 36 patients. In the final version, we achieved two-dimensional scanning of 10×10 cm^2 in 2 minutes, which covered the size of the majority of excised breast tumor tissues in lumpectomies [22]. To adapt to the tissue surface irregularity during the scanning, a collinear design was applied to fabricate the imaging probe (Figure S4), which was comprised of the ultrasound transducer, a fiber bundle, a pair of cylindrical lenses, and two glass slides. Light illumination from the imaging probe was consistent with the transport simulations (Figure S5) using ray-optics simulation toolbox from Matlab, demonstrating that the light from the end of the probe was collimated. With the collinear design, a fresh excised breast tumor tissue was imaged, showing 6 mm photoacoustic imaging depth and 13.4 mm adaptation, which was two times better than the traditional bifurcation design (Figure S6).

2.2. Development of an imaging protocol

A total of 30 female patients (Table S3) were enrolled in a study to determine the sensitivity and specificity of the multimodal ultrasound and PAT system. Patients requiring lumpectomy for diagnosis of breast cancer, including ductal carcinoma *in situ* (DCIS) and invasive ductal carcinoma (IDC) diagnosed by pre-operative imaging and core biopsies, were recruited at Indiana University Health Simon Cancer Center. All the patients signed and gave the informed consent for this study one day before the surgery per protocols approved by the Institutional Review Boards at Indiana University Health. Patients' names and other HIPPA identifiers were removed from all sections of the study.

In lumpectomy operation, after a tumor mass was resected, it was first oriented with a long suture marking the lateral margin and a short suture marking the superior margin. Then, it was placed on a sample tray, and transparent ultrasonic gel was applied on its surface for signal coupling (Figure 2A). The tray with gel coated specimen was inserted into the tissue scanner. The cover of the tissue scanner was then closed, and the gel contacted with a plastic film of a water reservoir. In the meantime, distilled water was automatically poured into the reservoir when the cover was closed. A series of 1,000 two-dimensional (2D) ultrasound/photoacoustic images (Figure 2B, C) were taken over a 10 by 10 cm^2 area within 2 minutes, and presented in three-dimensional (3D) layout (Figure 2D, E). Upon completion of the first imaging, the tissue was taken out from the scanner, flipped 180 degrees, and the aforementioned procedures were repeated to acquire the margin information of the other surface. With the automatic-scanning design, we minimized the whole procedure time to < 10 min. Finally, the tissue was cleaned and delivered to the histology room for further standard histopathology analysis. The researchers involved in the data acquisition were completely blinded to the final histology results.

2.3. Image analysis & evaluation protocol

All the ultrasound/photoacoustic images were acquired and processed with the same standard, and displayed in the same brightness level and contrast scale, as recommended by

board-certified radiologists with fellowship training in breast imaging. Data collected from the first enrolled 10 patients was used as a training set to establish the evaluation criteria. The representative images from the training data set including different features were shown in Figure 3. The first column (Figure 3A–D) showed the 2D ultrasound images, which indicated tumor mass (red ovals), micro-calcifications (bright spots inside the tissue, orange ovals), breast cyst (purple ovals), and fibrosis (blue ovals). The second column (Figure 3E–H) showed the 2D photoacoustic images, which mapped the adipose tissue (green ovals). All the images were confirmed by the corresponding hematoxylin and eosin (H&E) stained histology images (Figure 3I–L) in the third column [44,45]. Based on the latest consensus guidelines from Society of Surgical Oncology-American Society for Radiation Oncology-American Society of Clinical Oncology in 2016, IDC requires clear margin on ink and DCIS requires at least 2 mm clear margin from the tissue surface [23]. Therefore, for IDC, if it was not all covered by adipose tissue (no photoacoustic signals on the surface), it was considered a positive margin (Figure 4A–C), which was consistent with the current invasive breast margins guideline of margins on ink. For DCIS, if it was not all covered by adipose tissue with at least 2 mm thickness or micro-calcifications were found within 2 mm surface, it was considered a positive margin (Figure 4G–I). The margin assessment was made using the full set of ultrasound/photoacoustic images for each tissue. As long as at least one image frame showed abnormal, the tissue was deemed as positive in margin assessment.

2.4. Performance based on subjective reading

A blinded subjective reader study was performed to evaluate the statistical performance of the intraoperative multimodal ultrasound and PAT system. Data from the remaining 20 patients were used to calculate the sensitivity and specificity (Table 1) associated with the margin interpretation of the breast tumor tissues in the tissue/patient level. Three readers including an imaging researcher, a breast surgeon, and a board-certified radiologist were recruited for this study. The readers were firstly given a training set of sample ultrasound/photoacoustic images showing tumor mass, micro-calcifications, adipose tissue, and breast cyst to familiarize with the images acquired by the imaging system. Then, each reader was instructed to visualize the images of the 20 breast tissues and score the tissue on a scale of 1 to 4 as following: i) a score of 1 means that the reader is confident that the margin is negative for cancer; ii) a score of 2 means that the reader thinks that the margin is likely negative, but there is some uncertainty; iii) a score of 3 means that the reader thinks that the margin is likely positive, but there is some uncertainty; iv) a score of 4 means that the reader is confident that the margin is positive for cancer. After reading, the tissue margin was declared as negative only if given a score of 1 and positive if given a score of 2, 3, and 4, which represented a conservative clinical scenario. During the reading, each reader at first was instructed to evaluate the tissue margins by visualizing only ultrasound images of each tissue. Then, each reader was instructed to evaluate the tissue margins by visualizing ultrasound plus photoacoustic images of each tissue to judge whether the photoacoustic images would improve the reading results or not. Table 1 listed the statistical results for each reader. The results showed that only by ultrasound images itself, it was achieved 71.4% (95% CI, 30.3% – 94.9%) sensitivity and 76.9% (95% CI, 46.0% – 93.9%) specificity, 71.4% (95% CI, 30.3% – 94.9%) sensitivity and 53.9% (95% CI, 26.2% – 79.6%) specificity, and 71.4% (95% CI, 30.3% – 94.9%) sensitivity and 61.5% (95% CI, 32.3% –

84.9%) specificity for each reader. However, by ultrasound images plus photoacoustic images, it was achieved 85.7% (95% CI, 42.0% – 99.2%) sensitivity and 84.6% (95% CI, 53.7% – 97.3%) specificity, 71.4% (95% CI, 30.3% – 94.9%) sensitivity and 92.3% (95% CI, 62.1% – 99.6%) specificity, and 100% (95% CI, 56.1% – 100%) sensitivity and 53.9% (95% CI, 26.1% – 79.6%) specificity, respectively.

2.5. Performance based on machine learning

Subjective interpretation of the ultrasound/photoacoustic images by either breast surgeons or radiologists is time-intensive (10 to 15 min/tissue, 3 to 5 s/frame) and reader-biased. Consequently, a system which is able to rapidly deliver the consistent and accurate margin evaluation will be preferred during the breast-conserving surgeries. We employed a machine learning-based algorithm called deep convolutional neural network (CNN) for breast tumor margin assessment because it needed relatively less pre-processing and could achieve end-to-end supervised learning [46,47]. In this study, GoogLeNet Inception v3 CNN architecture was applied and adapted to the margin assessment through transfer learning. Based on the inception v3 architecture pre-trained on the ImageNet dataset, the original leaf nodes were firstly replaced with our own two-node (positive against negative). Then, the optimal threshold value for ultrasound model and photoacoustic model was obtained via the rule of farthest point from the diagonal in the Receiver Operating Characteristics (ROC) curve, respectively.

A training data set of 1052 positive frames and 918 negative frames was built by flipping and rotating the images generated by the multimodal PAT system. These frames were determined as positive or negative based on the reading of ultrasound and photoacoustic images by a trained radiologist, also they were correlated to pathology H&E staining read by a pathologist. Two independent CNN models were trained with only ultrasound and only photoacoustic data, separately. Then the two models were combined with an OR method, that was, an image was classified as positive if predicted as positive by either ultrasound model or photoacoustic model (Figure 5). A testing set was built with 76 positive frames and 70 negative frames, of which the margin status was declared by a board-certified radiologist. The ultrasound-only CNN model achieved a best sensitivity of 57.9% (95% CI, 46.0% – 69.0%) and specificity of 100% (95% CI, 93.5% – 100%) on margin assessment, with corresponding an area under curve (AUC) of 0.81. The photoacoustic-only CNN model achieved a best sensitivity of 77.6% (95% CI, 66.4% – 86.1%) and specificity of 90.0% (95% CI, 79.9% – 95.5%) on margin assessment with an AUC of 0.87. The ultrasound-photoacoustic-combined model achieved the best sensitivity of 85.53% (95% CI, 75.2% – 92.2%) and specificity of 90.0% (95% CI, 79.9% – 95.5%) on margin assessment, with corresponding an AUC of 0.93 (ultrasound threshold was fixed) or 0.88 (photoacoustic threshold was fixed).

2.6 Discussion

The goal of breast conservation surgery is to resect all cancer tissue while preserving as much normal tissue as possible for optimal cosmetic outcome. Achieving clear margin status of the excised breast tumor tissue, a key predictor of local recurrence [48,49], necessitates a fast and accurate intraoperative margin assessment tool. Current methods either need long

procedure time, or lack sensitivity and specificity. Here, we demonstrate an intraoperative multimodal ultrasound and PAT system for high-speed and accurate assessment of breast tumor margins in 20 patients.

The ideal intraoperative tool for tissue margin assessment should image the entire tissue surface in a fast manner. In breast conservation surgery, the excised tissue can be of arbitrary shape and large size, which usually has a tissue surface area ranging from 1 cm^2 to 100 cm^2. The tissue surface inevitably has a lot of fluctuations and irregularities, e.g. 10 mm height difference between tissue peaks and valleys. Conventional margin assessment tools, such as electrical resonance spectroscopy and OCT, have limited imaging depth of < 2 mm, and cannot adapt to such tissue surface fluctuation in scanning mode, which is significant to reduce the assessment time. To overcome this challenge, we developed two novel components. Firstly, our collinear imaging probe was able to provide 6 mm imaging depth and adapts to tissue surface fluctuation up to 13 mm. Secondly, we developed an imaging chamber that significantly simplified and shortened the tissue preparation time for ultrasound/photoacoustic imaging. For conventional scanning of a specimen, agarose gel solution is needed to be prepared beforehand, poured into a tissue container, naturally cures to fix the tissue, and water is later added to couple the signal from the tissue to the imaging probe. Such tissue preparation method is not only complex, but also time-consuming. Here, we designed a tissue cartridge and tissue container to prepare the tissue for scanning and reconstruct 3D images within 5 minutes in 4 steps: 1) Before the imaging, the fresh excised breast tissue is rinsed by 0.9% saline solution, which takes 1 minute; 2) Ultrasound gel is applied on the surface of the tissue, which takes less than 1.5 minutes (depending on the tissue size); 3) The tissue cartridge with the tissue was inserted into the imaging chamber, which takes less than 0.5 minute; 4) By pressing one button, the tissue surface was scanned within 2 minutes. Thus, the user was able to visualize the tissue margins of one surface within 5 minutes. In this study, two opposite faces were imaged for one tissue, taking less than 10 minutes, which was the fastest intraoperative breast tumor margin assessment tool to date. Also, 3D images of the breast tissue could be reconstructed, showing the tumor location and size. By correlating the suspicious area to the lumpectomy cavity, the surgeon will be able to locate the corresponding area of concern for future resection.

In the subjective reading, reader 1 achieved 71.4% (95% CI, 30.3% – 94.9%) sensitivity and 76.9% (95% CI, 46.0% – 93.9%) specificity only by ultrasound images, while 85.7% (95% CI, 42.0% – 99.2%) sensitivity and 84.6% (95% CI, 53.7% – 97.3%) specificity by ultrasound plus photoacoustic images. Reader 2 achieved 71.4% (95% CI, 30.3% – 94.9%) sensitivity and 53.9% (95% CI, 26.2% – 79.6%) specificity only by ultrasound images, while 71.4% (95% CI, 30.3% – 94.9%) sensitivity and 92.3% (95% CI, 62.1% – 99.6%) specificity by ultrasound plus photoacoustic images. Reader 3 achieved 71.4% (95% CI, 30.3% – 94.9%) sensitivity and 61.5% (95% CI, 32.3% – 84.9%) specificity only by ultrasound images, while 100% (95% CI, 56.1% – 100%) sensitivity and 53.9% (95% CI, 26.1% – 79.6%) specificity by ultrasound plus photoacoustic images. Apparently, different readers have distinct interpretation of thresholds for calling an image positive, and there is inter-reader variability (Cohen’s Kappa Coefficient between reader 1 and reader 2, between reader 1 and 3, and between reader 2 and 3 is 0.565, 0.340, and 0.205, separately). However, the most conservative reading still has a sensitivity of 71% and a specificity of 92%, which

is better than the current radio frequency spectroscopy (71% sensitivity and 68% specificity) and intraoperative X-ray (49% sensitivity and 73% specificity). The reported optical coherence tomography achieves 100% sensitivity and 82% specificity, but the decision criterion is margin on surface ink for all the tumor types in the reading. However, the new-released consensus guideline on breast margins requires at least 2 mm for DCIS, which leads to a sensitivity of only 63% for a recent clinical study [50] with the afore-mentioned optical coherence tomography probe because of its limitation in imaging depth. High frequency ultrasound itself provided a decent sensitivity in evaluating the breast tumor margins, especially in IDC specimens. However, with photoacoustic tomography, the detecting specificity of breast margins improved in IDC specimens, which would avoid unnecessary tissue excisions. Moreover, by adding the photoacoustic imaging channel, the multimodal ultrasound and PAT system improved both detection sensitivity and specificity for *in situ* cancer within 2 mm margins (Supplementary Table 4 – 6).

Machine learning-based algorithm may improve the speed, consistency and accuracy of margin assessment for breast conserving surgeries, intraoperatively. Our results have shown that CNN-based model achieved higher accuracy and adaptability than other automated approaches. The ideal CNN-based classification algorithm will require little pre-processing and provide general margin assessment for all tumor types in real time. The CNN-based classification algorithm reported here was able to distinguish between positive and negative margin status of 2 mm margin area for *in-situ* tumor at a speed of 0.7 s/frame. We anticipate that the accuracy of our classification algorithm can be further improved by: (1) collecting more patient data (including both positive and negative cases); (2) reducing background noise and fine-tuning parameters of image pre-processing. We also expect to obtain a more generalized classification algorithm that can be used for more types of breast tumors by: (1) training more CNN models focusing on different tumor types; or (2) adding another layer of pre-classifier before margin assessment.

3. Conclusion

As the prevalence of breast cancer screening, more lesions are identified in an early stage, leading to the popularity of using breast conservation surgeries. Achieving a negative or clear margin is essential for improving the clinical outcomes. However, an unmet need still exists to achieve time-efficient and highly-sensitive intraoperative evaluation of breast cancer margins during surgical procedures. Here, we demonstrate the first application of a customized mutlimodal ultrasound and PAT system for intraoperative breast tumor margins assessment using a compact and portable Raman-laser-based system and fresh lumpectomy specimens from 66 patients. Fresh lumpectomy specimens from a total of 36 breast cancer patients were used to improve the design, especially the collinear imaging probe and automatic tissue scanner. The final system provides three-dimensional compositional information of the entire excised breast tissue within 10 minutes. To evaluate the accuracy, fresh *ex vivo* human breast cancer tissues were obtained from 30 patients (10 for training, 20 for study), and imaged by the system maintained in a hospital surgical site. By subjective reading of three researchers, the results show 85.7% [95% CI, 42.0% – 99.2%] sensitivity and 84.6% (95% CI, 53.7% – 97.3%) specificity, 71.4% (95% CI, 30.3% – 94.9%) sensitivity and 92.3% (95% CI, 62.1% – 99.6%) specificity, and 100% (95% CI, 56.1% –

100%) sensitivity and 53.9% (95% CI, 26.1% – 79.6%) specificity respectively when cross-correlated with post-operational histology. Furthermore, a machine learning-based algorithm, termed deep convolutional neural network, was deployed for breast tumor margin assessment, and achieved 85.5% (95% CI, 75.2% – 92.2%) sensitivity and 90% (95% CI, 79.9% – 95.5%) specificity. Such results present the potential of using mutlimodal ultrasound and PAT as a high-speed and accurate method for intraoperative breast tumor margins evaluation.

4. Experimental Section

Clinical Study Design:

The objective of this study was to evaluate the potential of the multimodal ultrasound and PAT system to intraoperatively assess the breast tumor margin status in breast-conserving surgeries. Fresh excised human breast tumor tissues (n = 66) with different tumor types (IDC and DCIS) at Indiana University Health Simon Cancer Center were obtained and imaged by the imaging system. Patients undergoing mastectomies, or having infectious diseases, were excluded from this study. No patients were excluded based on age, ethnicity, race, or weight (Table S2). All the experiment protocols in this study were approved and carried out in accordance with the relevant guidelines and regulations.

Design of the Raman Laser:

A schematic of the compact $Ba(NO_3)_2$ based Raman laser was shown in Figure S2A, B. The Raman crystal was pumped by a Q-switched Nd:YAG laser at 10 Hz pulse repetition rate. A Faraday optical isolator was used to protect the Nd:YAG laser from the damage caused by back-scattering. A telescope composed of a planar-convex lens with 70 mm focal length and a planar-concave lens with −50 mm focal length was employed to shrink the beam size to match the dimensions of the $Ba(NO_3)_2$ crystal. For the Raman laser, a flat-flat resonator with a cavity length of about 10 cm was used. The resonator end mirror was coated with high reflectivity at 1197 nm (R > 99%), and high transmission at 1064 nm (T > 95%). The output coupler was coated with high reflectivity at 1064 nm (R > 99%) and 35% transmission at 1197 nm. The $Ba(NO_3)_2$ crystal, with dimensions of $7 \times 7 \times 90$ mm^3, was coated with high transmission at 1064 nm and 1197 nm on both faces.

The spectral profile of the generated Raman laser indicated the central wavelength of 1197.6 nm (Figure S2C), which lay in the second overtone absorption peak of lipid. The pulse duration of the output was measured to be 10.75 ns (Figure S2D), which met the thermal and stress confinements to efficiently generate photoacoustic signals. The maximum laser output could reach to 142 mJ when the pump energy was 294 mJ, corresponding a conversion efficiency of 48.3% (Figure S2E). The continuous laser power output within three hours was shown in Figure S2F. It indicated an average output of 1 W with 1.8% instability, which guaranteed sufficient pulse energy to excite the stable photoacoustic signals.

Design of the Automatic Tissue Scanner:

The automatic tissue scanner (Figure S3A) was capable of 2D scanning of 10×10 cm^2 area within 2 minutes. The integrated imaging probe was placed on the top cover. After each

breast conservation procedure, the top cover was lifted, and the fresh tissue was put on the tissue holder on the bottom (Figure S3B). Then, the top cover was closed, and a water reservoir covered with a plastic film contacted with the applied gel. Distilled water which was reserved in a water bottle was directed to the water reservoir as acoustic-coupling medium. The imaging head then performed a 2D scan of the tissue within the water reservoir (Figure S3C). After one surface scanning, the top cover was lifted, and the tissue was flipped for the other surface scanning. The whole procedure took < 10 minutes, which met the current economic need.

Design of the Collinear Imaging Probe:

The schematic of the collinear imaging probe was shown in Figure S4. It was comprised of a custom-built ultrasound transducer array, a fiber bundle, a pair of cylindrical lenses, and two glass slides. The laser light propagating from the fiber bundle went through one glass slide to the tissue surface to excite ultrasound signals. The generated signals were reflected by the two glass slides, and then received by the ultrasound transducer array. This collinear design was able to generate a collinear laser beam with a size of 2.6 mm x 10 mm at a distance of 10 mm (Figure S5), which was beneficial to adapt the tissue surface roughness. With a fresh excised breast tumor tissue, collinear design could reach 6 mm imaging depth with 13.4 mm adaptation, which was two times better than the traditional bifurcation design (Figure S6).

Histology Evaluation:

Based on the suture orientation, the fixed breast tumor tissue was first inked with different colors for the following margin identification. Then, it was grossed into several blocks. Through gross inspection, only suspicious areas from each block were incised and placed into a cassette for further standard H&E staining. Histology slides were digitized with a light microscope (ScanScope CS, Leica Inc.) at 20X magnification. Then all the H&E-stained histology images were interpreted by a board-certified pathologist for histopathologic assessment and margin status. The pathologist was blinded to the reconstructed images and results.

Supplementary Material

Refer to Web version on PubMed Central for supplementary material.

Acknowledgements

This work was partly supported by a Walther Cancer Foundation grant to Dr. Ji-Xin Cheng, and NIH STTR grant (1R41CA200006–01A1) to Vibronix, Inc. We thank the IUSCC Cancer Center at Indiana University School of Medicine, for the use of the Tissue Procurement and Distribution Core, which provided patient consent and tissue collection service. We also thank Charles R. Stine, Amanda M. Harshbarger, and Bradley W. Mosburg for breast tumor tissue grossing, Kyle McElyea, and Victoria Sefcsik for digitize tissue histology images, and Li-Hsin Tseng for analyzing acquired tissue images.

References

1. Siegel RL, Miller KD, Jemal A. Cancer statistics, 2016. CA Cancer J Clin, 66, 7–30 (2016). [PubMed: 26742998]

2. Fisher B, Anderson S, Bryant J, Margolese RG, Deutsch M, Fisher ER, et al. Twenty-year follow-up of a randomized trial comparing total mastectomy, lumpectomy, and lumpectomy plus irradiation for the treatment of invasive breast cancer. N Engl J Med, 347, 1233–1241 (2002). [PubMed: 12393820]

3. Veronesi U, Cascinelli N, Mariani L, Greco M, Saccozzi R, Luini A, et al. Twenty-year follow-up of a randomized study comparing breast-conserving surgery with radical mastectomy for early breast cancer. N Engl J Med, 347, 1227–1232 (2002). [PubMed: 12393819]

4. van Dongen JA, Voogd AC, Fentiman IS, Legrand C, Sylvester RJ, Tong D, et al. Long-term results of a randomized trial comparing breast-conserving therapy with mastectomy: European Organization for Research and Treatment of Cancer 10801 trial. J Natl Cancer Inst, 92, 1143–1150 (2000). [PubMed: 10904087]

5. Arriagada R, Le MG, Rochard F, Contesso G. Conservative treatment versus mastectomy in early breast cancer: patterns of failure with 15 years of follow-up data. Institut Gustave-Roussy Breast Cancer Group. J Clin Oncol, 14, 1558–1564 (1996). [PubMed: 8622072]

6. Jacobs L Positive margins: the challenge continues for breast surgeons. Ann Surg Oncol, 15, 1271–1272 (2008). [PubMed: 18320287]

7. Atkins J, Al Mushawah F, Appleton CM, Cyr AE, Gillanders WE, Aft RL, et al. Positive margin rates following breast-conserving surgery for stage I-III breast cancer: palpable versus nonpalpable tumors. J Surg Res, 177, 109–115 (2012). [PubMed: 22516344]

8. Balch GC, Mithani SK, Simpson JF, Kelley MC. Accuracy of intraoperative gross examination of surgical margin status in women undergoing partial mastectomy for breast malignancy. Am Surg, 71, 22–27; discussion 27–28 (2005). [PubMed: 15757052]

9. Fleming FJ, Hill AD, Mc Dermott EW, O'Doherty A, O'Higgins NJ, Quinn CM. Intraoperative margin assessment and re-excision rate in breast conserving surgery. Eur J Surg Oncol, 30, 233–237 (2004). [PubMed: 15028301]

10. Huston TL, Pigalarga R, Osborne MP, Tousimis E. The influence of additional surgical margins on the total specimen volume excised and the reoperative rate after breast-conserving surgery. Am J Surg, 192, 509–512 (2006). [PubMed: 16978962]

11. Riedl O, Fitzal F, Mader N, Dubsky P, Rudas M, Mittlboeck M, et al. Intraoperative frozen section analysis for breast-conserving therapy in 1016 patients with breast cancer. Eur J Surg Oncol, 35, 264–270 (2009). [PubMed: 18706785]

12. Cendan JC, Coco D, Copeland EM, 3rd. Accuracy of intraoperative frozen-section analysis of breast cancer lumpectomy-bed margins. J Am Coll Surg, 201, 194–198 (2005). [PubMed: 16038815]

13. D'Halluin F, Tas P, Rouquette S, Bendavid C, Foucher F, Meshba H, et al. Intra-operative touch preparation cytology following lumpectomy for breast cancer: a series of 400 procedures. Breast, 18, 248–253 (2009). [PubMed: 19515566]

14. Creager AJ, Shaw JA, Young PR, Geisinger KR. Intraoperative evaluation of lumpectomy margins by imprint cytology with histologic correlation: a community hospital experience. Arch Pathol Lab Med, 126, 846–848 (2002). [PubMed: 12088456]

15. Thill M MarginProbe: intraoperative margin assessment during breast conserving surgery by using radiofrequency spectroscopy. Expert Rev Med Devices, 10, 301–315 (2013). [PubMed: 23668703]

16. Thill M, Roder K, Diedrich K, Dittmer C. Intraoperative assessment of surgical margins during breast conserving surgery of ductal carcinoma in situ by use of radiofrequency spectroscopy. Breast, 20, 579–580 (2011). [PubMed: 21885281]

17. Goldfeder S, Davis D, Cullinan J. Breast specimen radiography: can it predict margin status of excised breast carcinoma? Acad Radiol, 13, 1453–1459 (2006). [PubMed: 17138112]

18. Erguvan-Dogan B, Whitman GJ, Nguyen VA, Dryden MJ, Stafford RJ, Hazle J, et al. Specimen radiography in confirmation of MRI-guided needle localization and surgical excision of breast lesions. AJR Am J Roentgenol, 187, 339–344 (2006). [PubMed: 16861535]

19. Nguyen FT, Zysk AM, Chaney EJ, Kotynek JG, Oliphant UJ, Bellafiore FJ, et al. Intraoperative evaluation of breast tumor margins with optical coherence tomography. Cancer Res, 69, 8790–8796 (2009). [PubMed: 19910294]

20. Keller MD, Vargis E, de Matos Granja N, Wilson RH, Mycek MA, Kelley MC, et al. Development of a spatially offset Raman spectroscopy probe for breast tumor surgical margin evaluation. J Biomed Opt, 16, 077006 (2011). [PubMed: 21806286]
21. Keller MD, Majumder SK, Kelley MC, Meszoely IM, Boulos FI, Olivares GM, et al. Autofluorescence and diffuse reflectance spectroscopy and spectral imaging for breast surgical margin analysis. Lasers Surg Med, 42, 15–23 (2010). [PubMed: 20077490]
22. Brown JQ, Bydlon TM, Richards LM, Yu B, Kennedy SA, Geradts J, et al. Optical assessment of tumor resection margins in the breast. IEEE J Sel Top Quantum Electron, 16, 530–544 (2010). [PubMed: 21544237]
23. Morrow M, Van Zee KJ, Solin LJ, Houssami N, Chavez-MacGregor M, Harris JR, et al. Society of Surgical Oncology-American Society for Radiation Oncology-American Society of Clinical Oncology Consensus Guideline on Margins for Breast-Conserving Surgery with Whole-Breast Irradiation in Ductal Carcinoma In Situ. Ann Surg Oncol, 23, 3801–3810 (2016). [PubMed: 27527714]
24. Pan H, Wu N, Ding H, Ding Q, Dai J, Ling L, et al. Intraoperative ultrasound guidance is associated with clear lumpectomy margins for breast cancer: a systematic review and meta-analysis. Plos One, 8, e74028 (2013). [PubMed: 24073200]
25. Doyle TE, Factor RE, Ellefson CL, Sorensen KM, Ambrose BJ, Goodrich JB, et al. High-frequency ultrasound for intraoperative margin assessments in breast conservation surgery: a feasibility study. BMC Cancer, 11, 444 (2011). [PubMed: 21992187]
26. Wang X, Pang Y, Ku G, Xie X, Stoica G, Wang LV. Noninvasive laser-induced photoacoustic tomography for structural and functional in vivo imaging of the brain. Nature Biotechnology, 21, 803–806 (2003).
27. Gateau J, Caballero MA, Dima A, Ntziachristos V. Three-dimensional optoacoustic tomography using a conventional ultrasound linear detector array: whole-body tomographic system for small animals. Med Phys, 40, 013302 (2013). [PubMed: 23298121]
28. Wang LV, Hu S. Photoacoustic tomography: in vivo imaging from organelles to organs. Science, 335, 1458–1462 (2012). [PubMed: 22442475]
29. Yao J, Wang LV. Photoacoustic tomography: fundamentals, advances and prospects. Contrast Media Mol Imaging, 6, 332–345 (2011). [PubMed: 22025335]
30. Cheng R, Shao J, Gao X, Tao C, Ge J, Liu X. Noninvasive Assessment of Early Dental Lesion Using a Dual-Contrast Photoacoustic Tomography. Sci Rep, 6, 21798 (2016). [PubMed: 26902394]
31. Wu J, You L, Lan L, Lee HJ, Chaudhry ST, Li R, et al. Semiconducting Polymer Nanoparticles for Centimeters-Deep Photoacoustic Imaging in the Second Near-Infrared Window. Adv Mater, 29, (2017).
32. Xi L, Grobmyer SR, Wu L, Chen R, Zhou G, Gutwein LG, et al. Evaluation of breast tumor margins in vivo with intraoperative photoacoustic imaging. Opt Express, 20, 8726–8731 (2012). [PubMed: 22513583]
33. Heijblom M, Piras D, van den Engh FM, van der Schaaf M, Klaase JM, Steenbergen W, et al. The state of the art in breast imaging using the Twente Photoacoustic Mammoscope: results from 31 measurements on malignancies. Eur Radiol, 26, 3874–3887 (2016). [PubMed: 26945762]
34. Ermilov SA, Khamapirad T, Conjusteau A, Leonard MH, Lacewell R, Mehta K, et al. Laser optoacoustic imaging system for detection of breast cancer. J Biomed Opt, 14, 024007 (2009). [PubMed: 19405737]
35. Diot G, Metz S, Noske A, Liapis E, Schroeder B, Ovsepian SV, et al. Multispectral Optoacoustic Tomography (MSOT) of Human Breast Cancer. Clin Cancer Res, 23, 6912–6922 (2017). [PubMed: 28899968]
36. Toi M, Asao Y, Matsumoto Y, Sekiguchi H, Yoshikawa A, Takada M, et al. Visualization of tumor-related blood vessels in human breast by photoacoustic imaging system with a hemispherical detector array. Sci Rep, 7, 41970 (2017). [PubMed: 28169313]
37. Dean-Ben XL, Fehm TF, Gostic M, Razansky D. Volumetric hand-held optoacoustic angiography as a tool for real-time screening of dense breast. Journal of Biophotonics, 9, 253–259 (2016). [PubMed: 25966021]

38. Wong TTW, Zhang R, Hai P, Zhang C, Pleitez MA, Aft RL, et al. Fast label-free multilayered histology-like imaging of human breast cancer by photoacoustic microscopy. Sci Adv, 3, e1602168 (2017). [PubMed: 28560329]
39. Wang B, Karpiouk A, Yeager D, Amirian J, Litovsky S, Smalling R, et al. Intravascular photoacoustic imaging of lipid in atherosclerotic plaques in the presence of luminal blood. Optics Letters, 37, 1244–1246 (2012). [PubMed: 22466209]
40. Cao Y, Hui J, Kole A, Wang P, Yu Q, Chen W, et al. High-sensitivity intravascular photoacoustic imaging of lipid-laden plaque with a collinear catheter design. Sci Rep, 6, 25236 (2016). [PubMed: 27121894]
41. Li R, Phillips E, Wang P, Goergen CJ, Cheng JX. Label-free in vivo imaging of peripheral nerve by multispectral photoacoustic tomography. J Biophotonics, 9, 124–128 (2016). [PubMed: 25904317]
42. Wang HW, Chai N, Wang P, Hu S, Dou W, Umulis D, et al. Label-free bond-selective imaging by listening to vibrationally excited molecules. Phys Rev Lett, 106, 238106 (2011). [PubMed: 21770549]
43. Li R, Slipchenko MN, Wang P, Cheng JX. Compact high power barium nitrite crystal-based Raman laser at 1197 nm for photoacoustic imaging of fat. J Biomed Opt, 18, 040502 (2013). [PubMed: 23536057]
44. Sharma T, Radosevich JA, Pachori G, Mandal CC. A Molecular View of Pathological Microcalcification in Breast Cancer. J Mammary Gland Biol Neoplasia, 21, 25–40 (2016). [PubMed: 26769216]
45. Sewell CW. Pathology of benign and malignant breast disorders. Radiol Clin North Am, 33, 1067–1080 (1995). [PubMed: 7480656]
46. LeCun Y, Bengio Y, Hinton G. Deep learning. Nature, 521, 436–444 (2015). [PubMed: 26017442]
47. Kuwahara M, Eiho S. [Image processing technics--focus on software. 1. Perspectives in biomedical image processing]. Iyodenshi To Seitai Kogaku, 21, 266–273 (1983). [PubMed: 6366293]
48. Dunne C, Burke JP, Morrow M, Kell MR. Effect of margin status on local recurrence after breast conservation and radiation therapy for ductal carcinoma in situ. J Clin Oncol, 27, 1615–1620 (2009). [PubMed: 19255332]
49. Houssami N, Macaskill P, Marinovich ML, Dixon JM, Irwig L, Brennan ME, et al. Meta-analysis of the impact of surgical margins on local recurrence in women with early-stage invasive breast cancer treated with breast-conserving therapy. Eur J Cancer, 46, 3219–3232 (2010). [PubMed: 20817513]
50. Zysk AM, Chen K, Gabrielson E, Tafra L, May Gonzalez EA, Canner JK, et al. Intraoperative Assessment of Final Margins with a Handheld Optical Imaging Probe During Breast-Conserving Surgery May Reduce the Reoperation Rate: Results of a Multicenter Study. Ann Surg Oncol, 22, 3356–3362 (2015). [PubMed: 26202553]

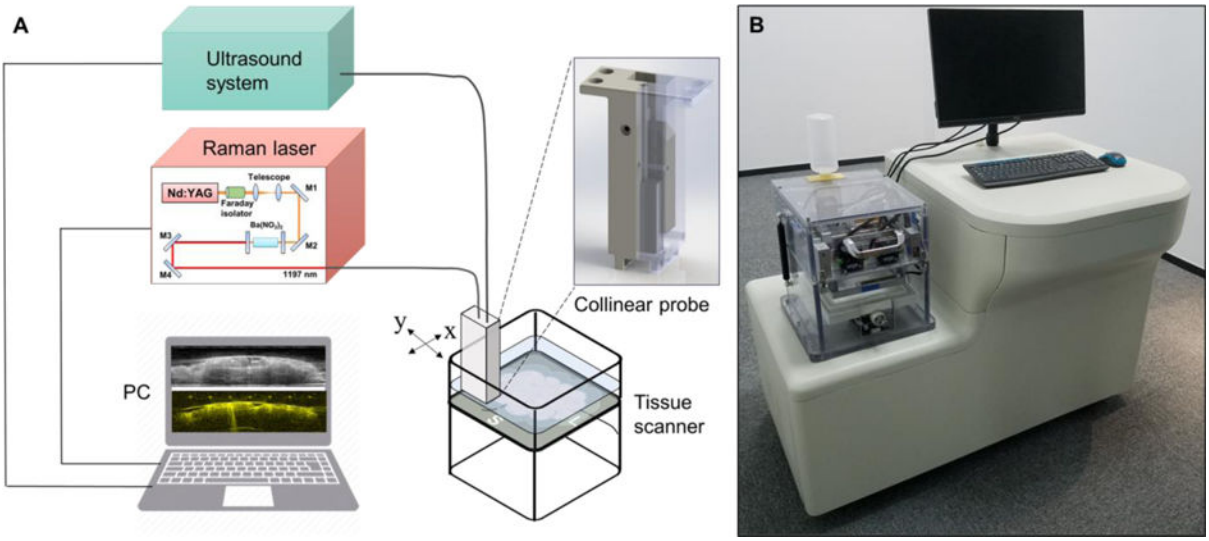

Figure 1.

Engineering an intraoperative multimodal ultrasound and PAT system. A) Schematic showing major components in the intraoperative multimodal ultrasound and PAT system. B) Illustration of the intraoperative multimodal ultrasound and PAT system.

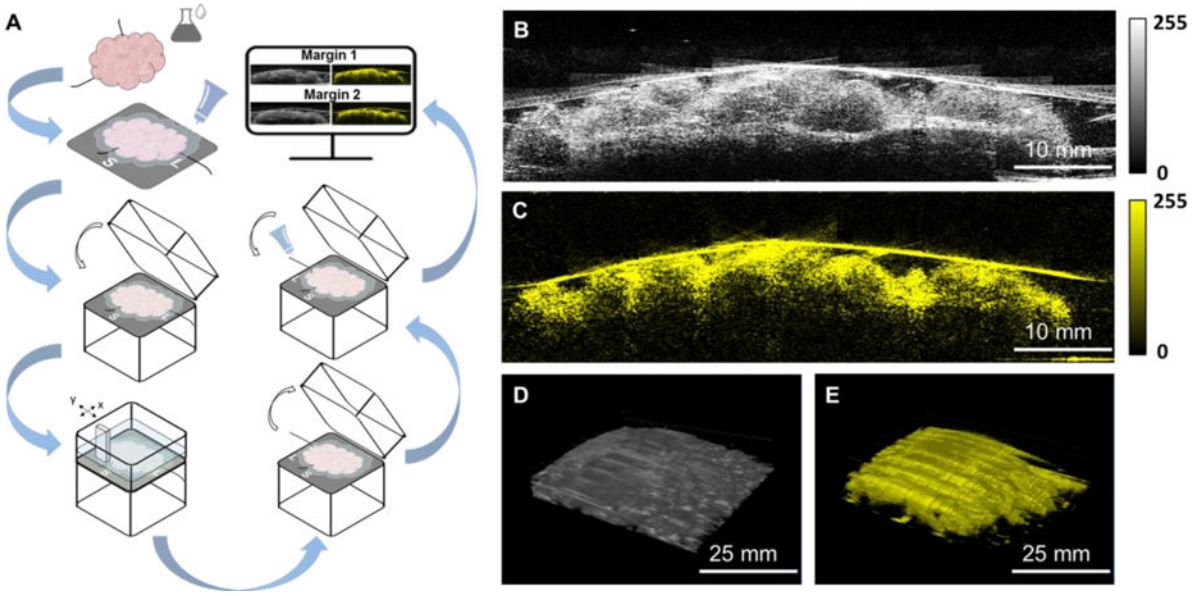

Figure 2.

Development of an imaging protocol. A) Imaging procedure. B) and C) Co-registered 2D ultrasound and photoacoustic images reconstructed by the multimodal ultrasound and PAT system. D) and E) Co-registered 3D ultrasound and photoacoustic images reconstructed by the multimodal ultrasound and PAT system.

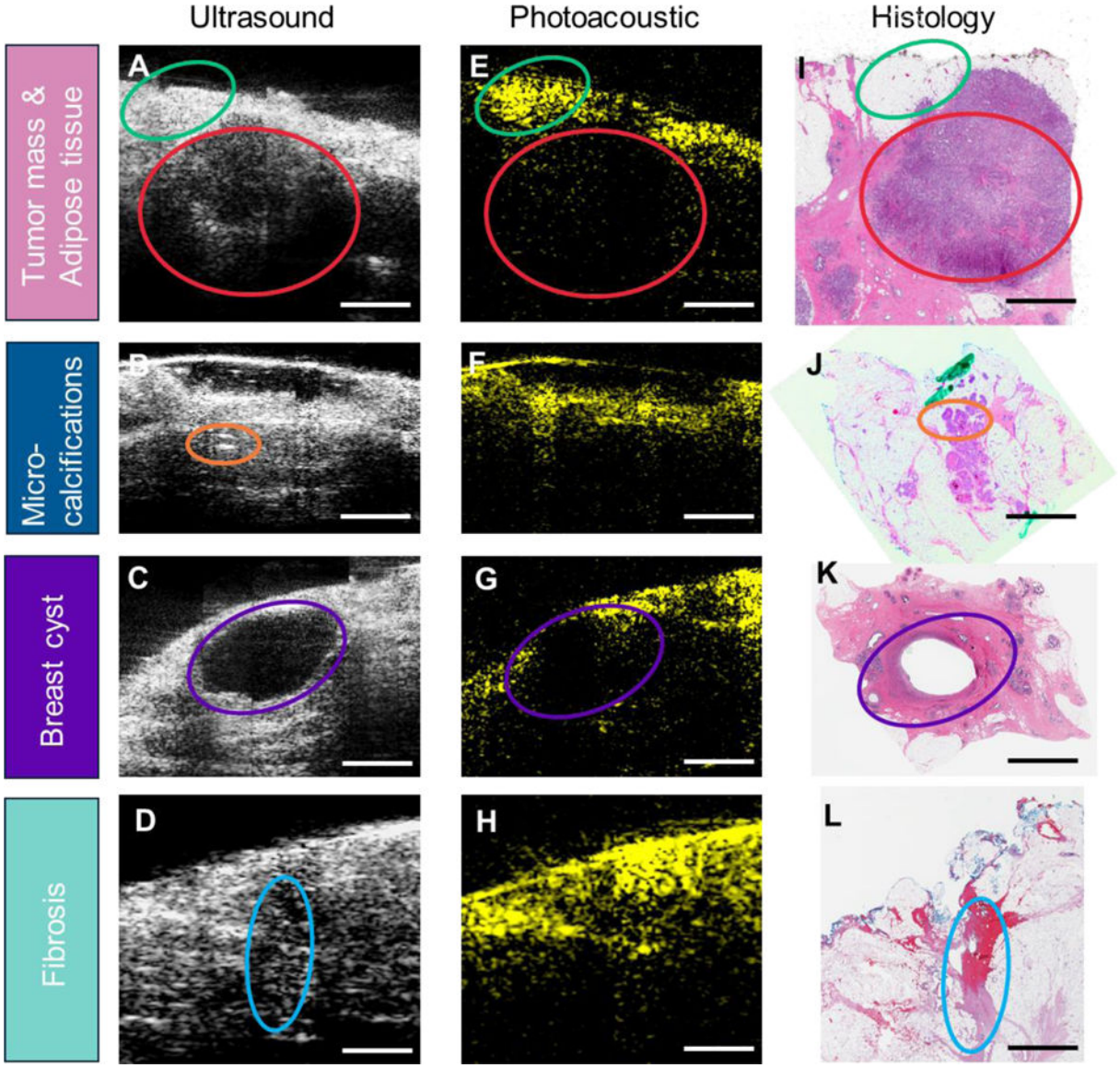

Figure 3.

Representative images showing different tissue features. A-D) 2D ultrasound images of breast specimen. E-H) 2D photoacoustic images of breast specimen. I-L) Corresponding H&E images of breast specimen. Adipose tissue is circled by green ovals. Tumor mass is circled by red ovals. Micro-calcifications are circled by orange ovals. Breast cyst is circled by purple ovals. Fibrosis is circled by blue ovals. Scale bar: 3 mm.

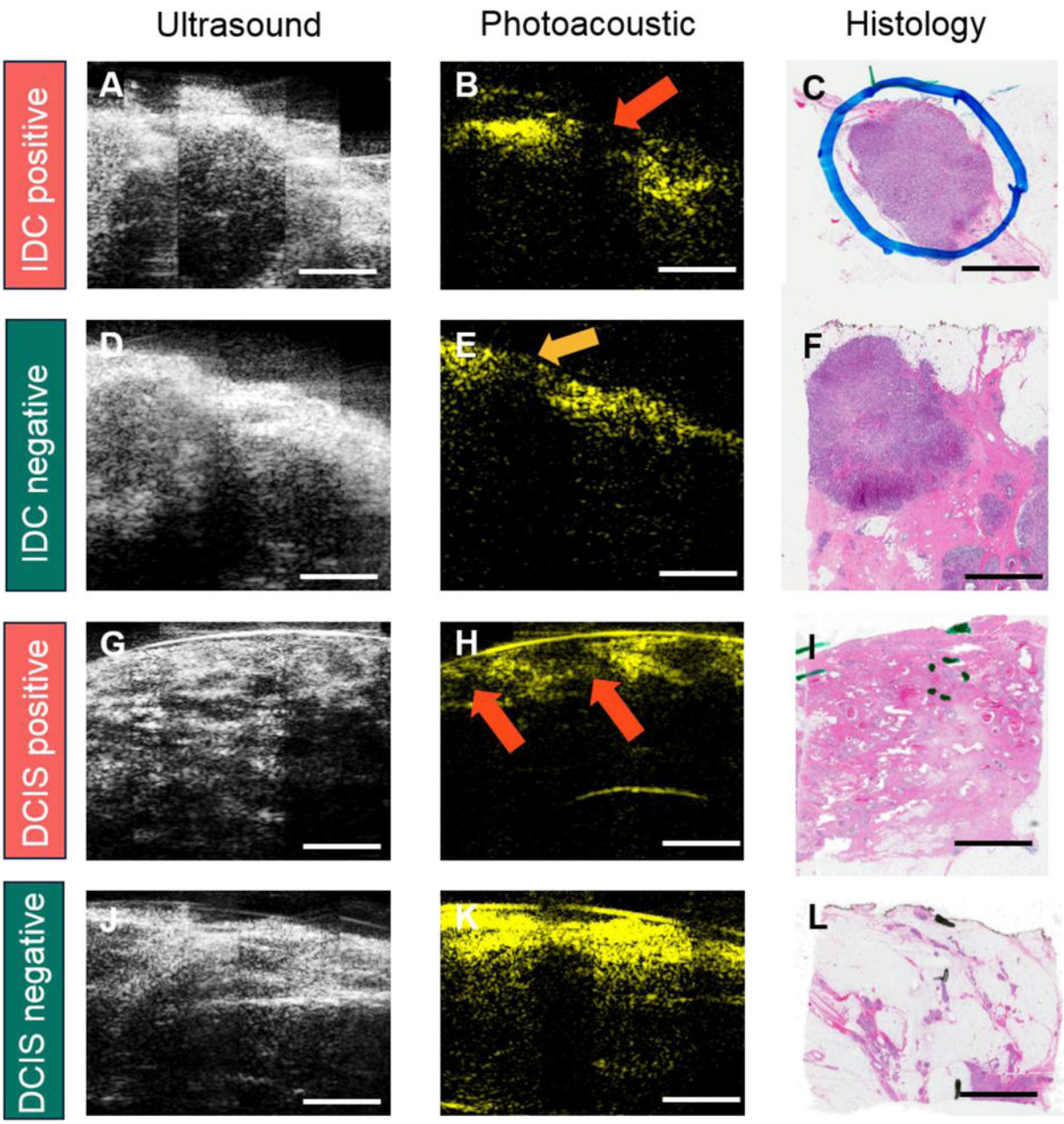

Figure 4.

Representative images of different margins from IDC and DCIS specimens. A-C) IDC positive margin with ultrasound, photoacoustic, and H&E images. D-F) IDC negative margin with ultrasound, photoacoustic, and H&E images. G-I) DCIS positive margin with ultrasound, photoacoustic, and H&E images. J-L) DCIS negative margin with ultrasound, photoacoustic, and H&E images. Red arrow in the first row indicates cancer protruding the margin. Orange arrow in the second row shows the cancer is covered by adipose tissue. The two red arrows in the third row indicate in-situ cancer covering by adipose tissue with the thickness less than 2 mm. Scale bar: 3 mm.

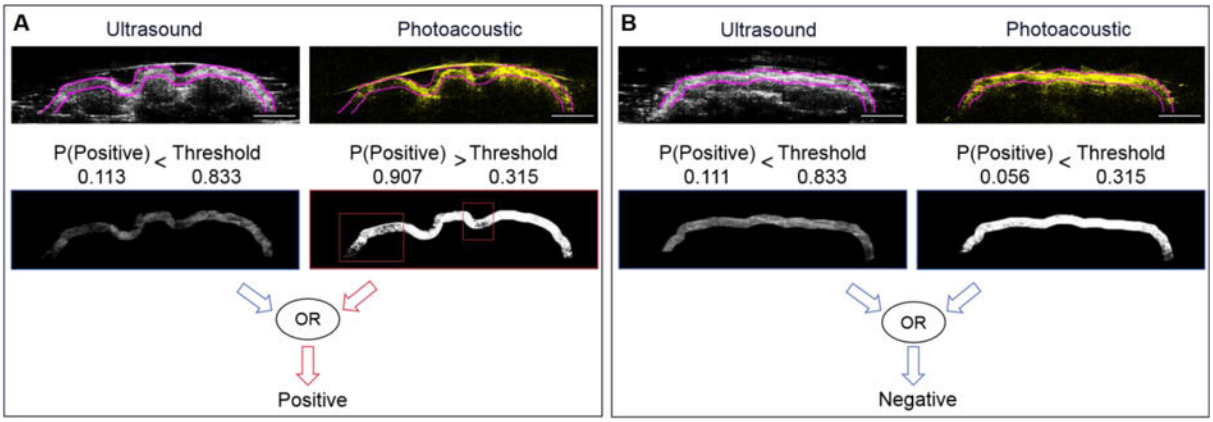

Figure 5.

Machine-learning based margin assessment. A) Illustration of positive margin. B) Illustration of negative margin. Scale bar: 5 mm.

Table 1.

Sensitivity and specificity by subjective reading analysis.

Reader	Statistics	Ultrasound only	95% CI	Ultrasound + Photoacoustic	95% CI
Reader 1	Sensitivity	71.4%	30.3% – 94.9%	85.7%	42.0% – 99.2%
	Specificity	76.9%	46.0% – 93.9%	84.6%	53.7% – 97.3%
Reader 2	Sensitivity	71.4%	30.3% – 94.9%	71.4%	30.3% – 94.9%
	Specificity	53.9%	26.2% – 79.6%	92.3%	62.1% – 99.6%
Reader 3	Sensitivity	71.4%	30.3% – 94.9%	100%	56.1% – 100%
	Specificity	61.5%	32.3% – 84.9%	53.9%	26.1% – 79.6%